

THE ANGLE-OF-SIGHT SIGNATURE FOR TWO-DIMENSIONAL SHAPE ANALYSIS OF MANUFACTURED OBJECTS

I. TCHOUKANOV,† R. SAFAEE-RAD,‡ K. C. SMITH†§|| and B. BENHABIB†§

† Department of Electrical Engineering, University of Toronto, 5 King's College Road, Toronto, Ontario, Canada M5S 1A4

‡ Computer Integrated Manufacturing Laboratory, Department of Mechanical Engineering, University of Toronto, 5 King's College Road, Toronto, Ontario, Canada M5S 1A4

§ Department of Mechanical Engineering, University of Toronto, 5 King's College Road, Toronto, Ontario, Canada M5S 1A4

|| Department of Computer Science, University of Toronto, 5 King's College Road, Toronto, Ontario, Canada M5S 1A4

(Received 24 September 1991; received for publication 14 February 1992)

Abstract—A new two-dimensional (2D) shape-encoding scheme is introduced which is based on the idea of the angle-of-sight (AOS). Using this scheme, a shape can be efficiently transformed into a one-dimensional (1D) signature by recording the AOS vs. distance of each boundary point with respect to a shape-specific chord-of-sight (COS). The COS is selected by using an extension of the notion of shape boundary, to the idea of shape-specific points and the characteristic ellipse (CE). The AOS signature has many important properties including: it is information-preserving and thus unique, it does not require boundary smoothing; it has its own selectable smoothing property; it can provide a set of multi-scale representations by means of a simple operation; it is transformation-invariant; it is defined at all points; it preserves symmetries. As well, for matching purposes, a two-level matching process is proposed using a global measure (the eccentricity of the CE of a shape) and a dissimilarity measure based on the AOS signature. The encoding and matching techniques developed have been tested with 35 manufactured objects. The results obtained show that the AOS signature and the two-level-matching technique are quite effective and reliable for the recognition of 2D shapes of typical manufactured objects.

Shape analysis Shape encoding Signature Shape matching Shape-specific properties

1. INTRODUCTION

Shape representation and matching is a key problem in machine-vision-system development. This problem arises, as well, in the context of a new active-vision system for three-dimensional (3D) object recognition in robotic assembly workcells, under development in the Computer Integrated Manufacturing Laboratory (at the University of Toronto).^(1,2) In the latter development, the main design concept is to reduce the dimensionality of the recognition task: a 3D object is modeled in this system by using a small set of topologically distinct perspective views, called *standard views*. The process of shape matching is performed between the acquired two-dimensional (2D) standard view of the sensed object with unknown identity and a library of 2D standard views of a set of objects. Based on the proposed method, then, any usable 2D representation and its corresponding recognition technique must be *position-, rotation-, and scale-invariant*.

Here, following the same concept of dimensionality reduction in a "top-down" fashion, the problem of the design of a transformation-invariant 2D shape-encoding scheme is addressed. Our goal has been the identification of a methodology by which the 2D standard views are transformed into one-dimensional

(1D) signatures suitable for signal matching. Here the required signature is defined as a 1D signal derived from the shape by using an encoding scheme for mapping the information from the 2D "shape" space to the 1D "signature" space.

The general problem of 2D shape recognition (classification/discrimination) is one of the most familiar and fundamental problems in pattern recognition. Shape analysis, generally, consists of two basic processes: *shape representation* (description/modeling/encoding) and *shape identification* (matching). Clearly, to a certain extent the type of matching technique employed is determined by the method of shape representation used. In the last three decades, various methodologies have been developed to address this problem in various contexts. These methods have been reviewed and classified in a number of papers.⁽³⁻⁵⁾

In the proposed 2D shape-recognition technique for representation/encoding purposes, a new boundary-based signature is developed and used. The new 2D shape-encoding scheme is based on a new concept, the angle-of-sight (AOS), for extracting and encoding "shape" information.⁽⁶⁾ Parameterization of the boundary of a 2D shape provides a 1D representation (signature) of the geometrical information (which is a periodic function of one variable). This has several

advantages: it allows a more compact representation of 2D shapes; it enables one to apply various well-developed theoretical techniques (e.g. Fourier analysis) to generate even a more compact representation and scalar-measure-based identification of 2D shapes; and, it can facilitate shape analysis in general. As a result, it is a quite attractive approach for image-data compression and shape analysis. Various 2D shape-boundary parameterization methods have been proposed either as an *intermediate* representation—either for subsequent transformations (such as Fourier transform) in order to get a set of scalar features, or for subsequent processing for extraction of structural primitives of the boundary, or as a *final* form of representation (for direct matching). These parameterization techniques include: the polar representation,^(7–9) the centroidal profile representation,^(10–14) the rectangular representation,^(15–17) the tangential representation,⁽¹⁸⁾ the curvature representation,^(19–22) the normal-contour-distance (NCD) signature,⁽²³⁾ the slope density description,⁽²⁴⁾ “signature”,^(25,26) the angle-and-length chord distribution,^(27–31) and the gradient encoding scheme.⁽³²⁾

The proposed 2D shape-representation technique is based on the parameterization of the boundary as a periodic function of one variable (a signature), and has the following properties. It is easily computed from a chain code and thus has a low processing/memory requirement; it is information-preserving and thus unique; it does not require boundary smoothing since it is not based on first or second derivatives of the boundary; it has its own inherent smoothing property; it can provide a set of multi-scale representations by means of a simple operation; it is position-invariant, rotation-invariant (through standardization of a starting point), and size-invariant (through a simple normalization of the perimeter length—the signature is required to be normalized only along *one* axis); it is a single-valued function, defined at all points, and does not have abrupt changes in the signature amplitude (and thus has an inherent smoothing property); the shape of each object is encoded by only one function (the signature) as opposed to two (as in the rectangular representation); it preserves symmetries; it represents deviation from a basic shape (the circle), and as a result, it can be used for creating a measure to test circularity; and, it is a stable representation in the sense that small changes in the boundary will have a small effect on the signature.

The proposed representation scheme suffers from two basic drawbacks: (1) it cannot be applied to occluded or partially visible shapes (open curves), although, in the proposed 3D object-recognition system, this situation does not occur; and, (2) since it is based on chain code (using link lengths of 1 or $\sqrt{2}$), the boundary is not uniformly sampled; as a result, at different orientations, a shape will yield different signatures since the path length is longer in the diagonal directions. In fact, the maximum factor of change in the Freeman-chain-coded perimeter length of a shape

(in *link* units) due to rotation can be as high as $\sqrt{2}$. A number of papers have addressed the variation of perimeter length of 2D shapes due to digitization errors in general,⁽³³⁾ and under Freeman chain coding in particular.⁽³⁴⁾ If necessary, the non-uniformity of sampling of the boundary can be removed by applying uniform sampling techniques developed for digitized curves.^(23,35)

On the whole, the above-mentioned properties make the proposed encoding technique attractive for shape representation and suitable for shape matching, and thus, for 2D shape analysis in general.

In Section 2, the new 2D shape-encoding scheme, which is based on the idea of the AOS, is introduced. In Section 3, the properties of the new AOS signature are discussed. Matching of AOS signatures is addressed in Section 4. Experimental results, for simulated as well as real 2D shapes, are presented and analyzed in Section 5. A brief summary is given in the final section, Section 6.

2. THE PROPOSED BOUNDARY-BASED 2D SHAPE-REPRESENTATION TECHNIQUE

In this paper, “shape” is defined as a simply connected compact region in a 2D Euclidean space, which may or may not be convex.⁽²⁸⁾ The set of boundary or frontier points of this region are used to characterize its shape. Only manufactured objects are considered here since their construction is based on definable specifications (objects encountered in manufacturing plants, storage and sorting facilities, cars, ships, airplanes, and spacecraft). What characterizes such objects is their geometry: their surfaces are mathematically well defined by planes, cylinders, cones, etc., or otherwise by splines, contour lines, and so on. Due to the above-mentioned characteristics, their representation and identification are relatively simpler than those for natural shapes, and consequently can be potentially more successful.

2.1. Description of the AOS shape-representation scheme

The angles of a triangle formed by any three non-colinear boundary points C, D and E of a 2D shape (Fig. 1) are invariant under shape translation, rotation and scaling. The following thought experiment can be performed to visualize the use of this property in a shape-encoding scheme: *predetermine* two of the vertices, say C and D, and keep them fixed while moving the third vertex E along the shape’s boundary (Fig. 1). The angle α , associated with each position of the moving vertex E, is a descriptive property of the boundary and can be used for shape representation. Hereafter, the chord joining the fixed points is referred to as the chord-of-sight (COS) and the angle α formed at the third vertex is referred to as the AOS.

The AOS signature is a boundary-based descriptor of a planar shape and defined as a 1D signal $AOS = \alpha(l)$, where l is the arc length between a starting point E_0

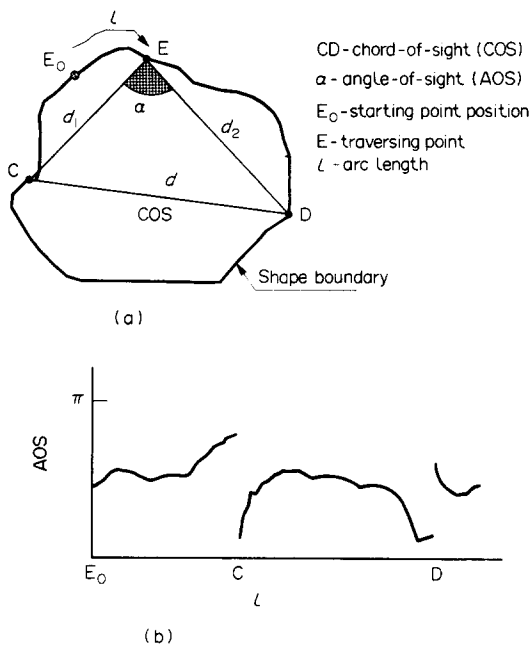


Fig. 1. (a) Definition of the AOS. (b) The derived signature.

and the boundary-tracing point E in the clockwise (or counterclockwise) direction

$$\alpha(l) = \arccos \left[\frac{d_1^2(l) + d_2^2(l) - d^2}{2d_1(l)d_2(l)} \right], \quad \alpha(l) \in (0, \pi) \quad (1)$$

where $d_1(l)$ and $d_2(l)$ are the distances from the tracing point to the end-points of the COS, and d the length of the COS.

The AOS signature of a planar shape with *normalized boundary length* has the following properties:

- it is translation-invariant;
- it is size-invariant;
- it is a periodic signal, and thus, a change of the starting-point position causes only a cyclic shift of the signature;
- it is computationally inexpensive, since its computational cost is linearly proportional to the number of boundary points (N), that is, it is $O(N)$.

In order to make the signature rotation-invariant as well, its starting point must be standardized. In that respect, the AOS encoding scheme uniquely defines an orthogonal shape-specific coordinate system, which can be used to select a "standard" starting point E_0 . The geometry of this situation can be studied using Fig. 2. The loci of boundary points having one and the same AOS are circular arcs passing through the end-points of the COS. The locus of the centers of these constant AOS arcs is a straight line orthogonal to the COS and passing through its midpoint. The intersection points of this line and the boundary are object-specific points, and each can be used as the starting point for the AOS signature. To make the starting point unique, the most distant (or the least distant) intersection point

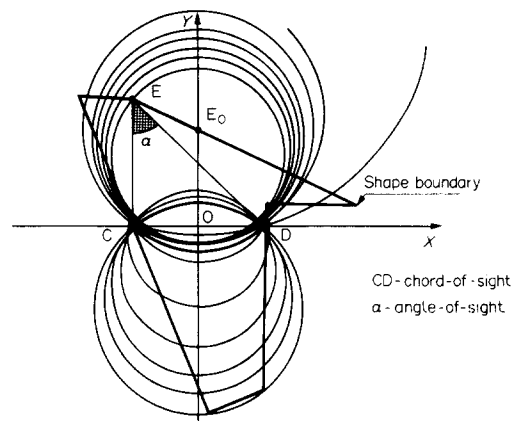


Fig. 2. The AOS related coordinate system.

to the origin of the shape specific coordinate system (point O in Fig. 2) can be used. If there is more than one such point (typically a rare case for industrial shapes), then a like number of shifted signatures must be derived. Subsequent to standardization of the starting point E_0 , the AOS signature becomes rotation-invariant as well.

2.2. COS selection requirements

The AOS encoding scheme implies that the positions of the COS end-points are *predetermined* by an off-line selection process, whereas their locations are detected in real time. Obviously, the AOS signature of a shape is transformation-invariant only if one and the same pair of COS end-points is unambiguously detected for each position, orientation, and size of the shape. As far as the shape-recognition problem is concerned, matching AOS signatures is to be performed only if they are derived with reference to a COS with one and the same identity. Therefore, COS selection requirements must be established. The COS end-points must have the following properties:

- *Uniqueness*: the COS end-points must be uniquely identifiable from the shape boundary (or features derived from it).
- *Commonality*: the COS end-point determination must rely on features common to a given set of shapes.
- *Boundary-distortion tolerance*: the COS end-points must be chosen so as to be minimally sensitive to boundary noise.
- *Detectability*: the COS end-points must be identified fast and readily.

The last requirement is in contradiction with the first three. The first three can be satisfied by points having a large domain of support. However, as a consequence, detection of such prominent points (in a pointwise sense) would require considerable computational time. Points relying on a local domain of support, such as corners, dominant points, etc., can hardly meet the above-stated requirements. Generally,

the end-points of the longest boundary primitives, such as linear or curved segments, are better candidates for the COS end-points, but their detection requires considerable processing time.^(36,37)

Ideally, the best candidates for the COS end-points are points to whose coordinates all boundary points collectively contribute.

2.3. COS based on shape-specific points

The concept of shape-specific points is an extension of the notion of shape to include points which do not lie on the shape boundary. The formal definition of a shape-specific point is given in reference (38), and for the sake of clarity, it will be repeated here:

“Let $p = F(S)$ be a point computed from shape S according to procedure F . Also, let $S' = T(S)$, where T is a planar transformation, (translation, rotation, or dilation), and let $p' = F(S')$. Then p is a shape-specific point of S with respect to transformation T if and only if $p' = T(p)$.”

This definition also applies to geometrical entities other than points. For instance, the length of a chord connecting two shape-specific points is shape specific as well.

Shape-specific points have several properties which make them attractive to the AOS encoding scheme:

- Shape-specific points behave as if they were on the shape boundary.
- The coordinates of shape-specific points are computed rather than detected.
- All boundary points collectively contribute to the computation of the coordinates of shape-specific points. In this sense, the whole shape's boundary acts as a domain of support for each shape-specific point.

An AOS signature derived with respect to a COS, which is based on shape-specific points, retains the property of being shape-transformation-invariant (as was explained in Section 2.1). The method for selection of the starting point of a signature, presented in Section 2.1, is applicable to shape-specific COS end-points as well.

Various functions can be defined for shape-specific-point computation. Mitiche and Aggarwal⁽³⁸⁾

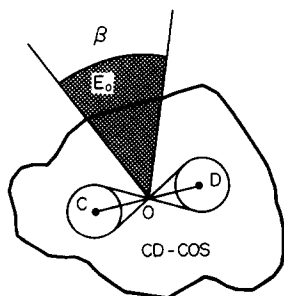


Fig. 3. Noise-induced shift of the signature starting point.

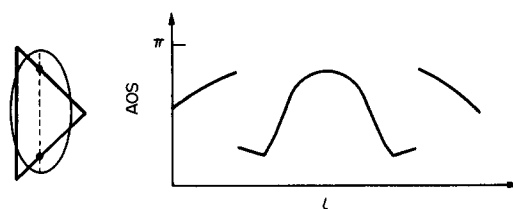


Fig. 4. The AOS signature of a triangle.

employed the centroid and the weighted median point to recover shape orientation for the purpose of registration. However, simulated experiments here have indicated that boundary noise causes a significant shift in the starting point position of the corresponding AOS signature when these two points are used to define the COS. This is explained by the geometry in Fig. 3, where the COS end-points are shown to be affected by isotropic noise with standard deviation ϵ . The shift of the signature-starting-point position lies within an angular interval determined by the following formula:

$$\beta = 2 \arcsin\left(\frac{2\epsilon}{d}\right). \quad (2)$$

This formula suggests that the noise-induced shift of the AOS signature starting point is decreased by increasing the length of the COS, d . The distance between the centroid and the weighted-mean point of a compact shape is usually small, a fact which deteriorates the noise-tolerance of the corresponding AOS signature.

In view of the above consideration, better results can be achieved by using shape-specific points which are computed from a Fourier expansion of the rectangular representation of a shape. Kuhl and Giardina⁽¹⁵⁾ have applied a Fourier trigonometric expansion to the X and Y projections of a closed contour and have shown that the locus of each vector of constant frequency is elliptical. The five basic parameters of the ellipse related to the fundamental Fourier harmonic are given in reference (39). It has been proven here that this ellipse is shape specific (as presented in the Appendix). Thus, it can be said that this shape-specific ellipse is an important extension of the notion of shape. Hereafter, the shape-specific ellipse related to the first harmonic (the fundamental frequency) will be referred to as the characteristic ellipse (CE). As an example, the AOS signature of a triangle is shown in Fig. 4. The crossing points of the shape boundary and the major axis of the CE are used as the COS end-points.

2.4. An improved 3D based AOS encoding scheme

The AOS function is not defined for boundary points which are collinear with the end-points of the COS, and therefore, the associated signature suffers from having jump discontinuities for such points. Jump discontinuities hinder matching of signatures and deteriorate the spectral characteristics of the

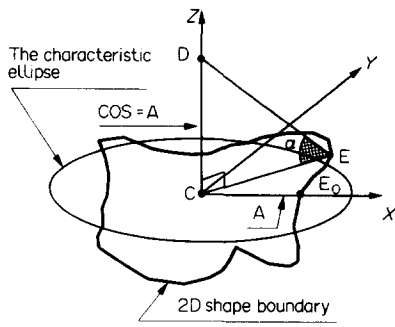


Fig. 5. Definition of an improved AOS scheme.

signal (through Gibbs' phenomenon). This is a common drawback of many boundary-based encoding (signature) schemes.⁽⁵⁾

This problem can be solved by placing one of the end-points of the COS outside of the plane of the "image". An orthogonal XYZ frame is considered herein to achieve this (Fig. 5), where the origin co-

incides with the center of the characteristic ellipse of the boundary, and the X and Y axes are aligned with its major and minor radii. The length of the COS is defined to be equal to the major (or minor) radius of the characteristic ellipse of the boundary. In the same manner as in Section 2.1, the AOS signature is defined as a 1D signal $AOS = \alpha(l)$, where l is the arc length between the moving point E and a starting point E_0 , measured in a clockwise (or counterclockwise) direction. Note that, as a result of employing the third dimension, the AOS function has no discontinuities. Based on this new definition of COS, the AOS function is defined as follows:

$$\alpha(l) = \arctan \left[\frac{A}{r(l)} \right], \quad \alpha(l) \in (0, \pi/2) \quad (3)$$

where A is the length of the major radius of the characteristic ellipse of the boundary (the minor radius B of CE can be used as well), and $r(l)$ is the distance from a boundary point to the origin of the XYZ frame. The crossing point of the boundary and the Y-axis or

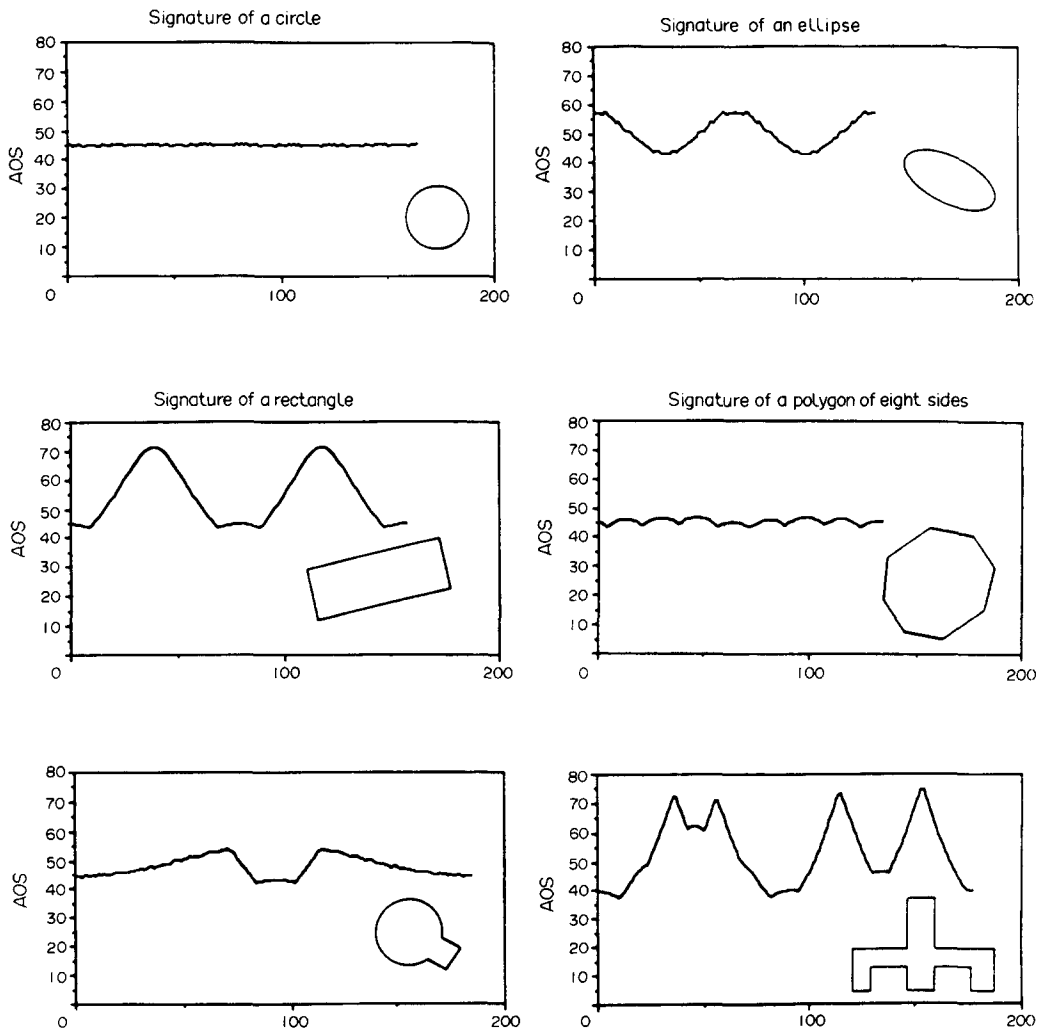


Fig. 6. AOS signatures of a set of simulated shapes.

X -axis (which are respectively aligned with the major and minor axes of the characteristic ellipse of the shape), which is the most distant (or least distant) from the origin of the XYZ frame, can be used as a "standard position" for the starting point.

Figure 6 shows a set of simulated shapes and their AOS signatures as proposed in this section.

3. THE PROPERTIES OF THE AOS SIGNATURE

The improved version of the AOS encoding scheme has the following important properties:

- It can easily be computed from a chain code and has a low processing/memory requirement.
- The signature preserves shape symmetry in the sense that points equidistant from the origin of the XYZ frame have equal AOS.
- It is inherently position-invariant, and, through standardization of the starting point, it is easily made rotation-invariant. Furthermore, by normalizing the boundary length of a shape, the signature becomes size-invariant as well.
- The signature is a single-valued function, defined at all points, and does not yield abrupt changes in the signature amplitude due to its inherent smoothing property (Section 3.1).
- The simplest possible signature (a straight line) belongs to the circle—the basic shape. In this sense, the AOS signature shows how a shape deviates from the basic shape. This property can be used to define a new measure-for-circularity test.
- The problem of oversampling/undersampling of the boundary for the AOS signature is significantly less severe than similar encoding techniques such as polar representation, since the signature is based on contour sequence (Freeman chain code). Experimental results in Section 5 will show how significant this problem is for the proposed signature in practice.
- It is a stable representation, since small changes in the boundary will have small effects on the signature (thus it is stable under noise such as that from quantization). A reason for this is the inherent smoothing property of the proposed encoding scheme (Section 3.1). This property will be illustrated more clearly by the experimental results (with simulated as well as real test shapes) in Section 5.

In the following sections, three other important properties of the AOS signature will be discussed in detail.

3.1. The smoothing property of the AOS signature

Representation techniques based on first derivatives (i.e. slope) or second derivatives (i.e. curvature) of the boundary of a shape are very sensitive to boundary noise, and as a result, they require an initial smoothing process before a signature is generated. This requirement generates another problem, namely, the extent to which the boundary should be smoothed in order to

get a reliable representation (since, obviously, the scale at which the smoothing is carried out has a significant effect on the behavior of the boundary). This is an important problem in image processing and analysis, and there is no general and easy solution to it. Thus, encoding schemes such as tangential representation, curvature representation, NCD signature, slope-density function, and gradient encoding scheme all suffer from this important drawback. Furthermore, the preprocessing operation increases computational costs of the representation. As well, due to the above preprocessing, in general, they do not have the information-preserving property.

As noted already, one of the important advantages of the proposed encoding scheme is that it provides an inherent smoothing of the shape representation, since the amplitude of the transfer function $y = \arctan(x)$ is always under the line $y = \pi/2$. That is, as the value of the variable x increases, the rate of change of the function value y is reduced by the above transfer function, and y becomes asymptotically closer to the limiting value $\pi/2$. As well, the signature can easily be further smoothed by increasing the length of the COS. This latter property can be employed selectively for boundary-noise reduction. A family of AOS signatures of a shape presented in Fig. 7 shows that a longer COS causes smoothing of the form of the signal and an increase in its DC component. Now, if a family of signatures is translated along the y -axis to a position having a fixed DC component value (e.g. $\pi/4$), then they can be viewed as signatures of the shape with different degrees of smoothing. From a geometrical point of view, through this process of smoothing, the boundary of a shape gets closer to the ideal smooth shape (the circle).

3.2. The shape-preserving property of the signature

The AOS signature preserves shape information. In general, signatures from which shape can be recovered

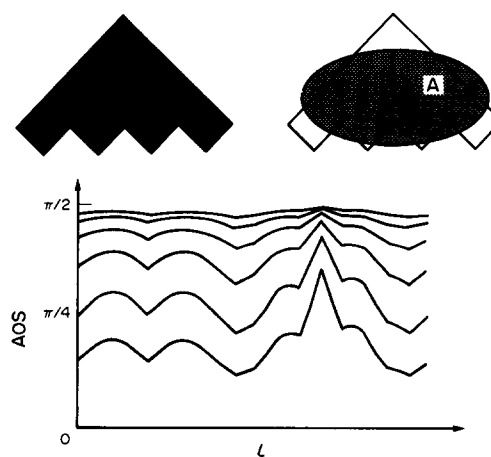


Fig. 7. A shape and the corresponding family of AOS signatures for various lengths of COS: 0.5 A , 1 A , 2 A , 4 A , 8 A , and 16 A .

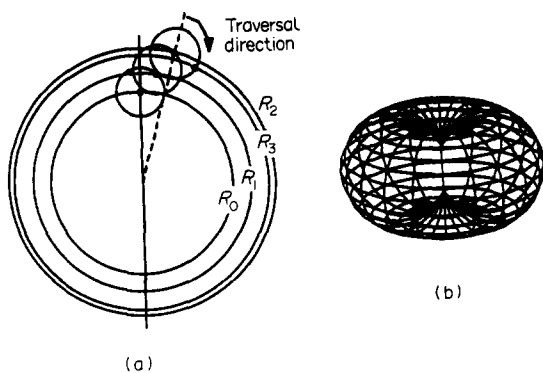


Fig. 8. (a) Shape recovery from the improved AOS signature. (b) 3D locus of constant AOS points.

are referred to as information-preserving signatures.⁽⁴⁾ To prove this property, it is sufficient to show a procedure performing the “shape-from-representation” transform. Figure 8(a) shows the geometry of such a shape-recovery transform. The AOS signature is defined by a discrete sequence $AOS(i) = \alpha(l_i), i = 0, 1, \dots, N - 1$ (where N is the total number of elements in the sequence; e.g. the total number of links in the Freeman-chain-coded boundary of a shape), parameterized with respect to the arc length l . The 3D locus of all points having constant AOS is the surface of a toroid (a surface of revolution generated by rotating constant-AOS arcs around the COS—Fig. 8(b)). The intersection of the i th AOS toroidal locus with the image plane is a circle (Fig. 5) of radius

$$R_i = \frac{A}{\tan(AOS(i))} \quad (4)$$

where A is the length of the COS. Consequently, a shape-recovery procedure can be described as follows:

- (1) for $i = 0$ to $N - 1$ draw concentric circles with radius R_i ;
- (2) choose an arbitrary starting point P_0 , lying on the first circle (R_0);
- (3) for $i = 1$ to $N - 1$, draw a circle centered at point P_{i-1} with radius $\Delta l_i = l_i - l_{i-1}$ (for a boundary encoded by Freeman chain code, the length Δl_i would be equal to 1 or $\sqrt{2}$). The boundary points P_i are recovered by taking the crossing points of this circle and a circle of radius R_i in the *direction of traversal* (clockwise, in our case).

In step (3) above, since the intersection of the two circles generally yields two solutions, one of them must be selected. The proper selection of the solution depends on convexity–concavity of a shape. In this regard, there exist three possible cases:

- (a) For a convex shape, the condition stated in step (3) above always results in the correct recovery of the shape.
- (b) For some convex–concave shapes (e.g. Fig. 9(a)), the above criterion works directly as well.

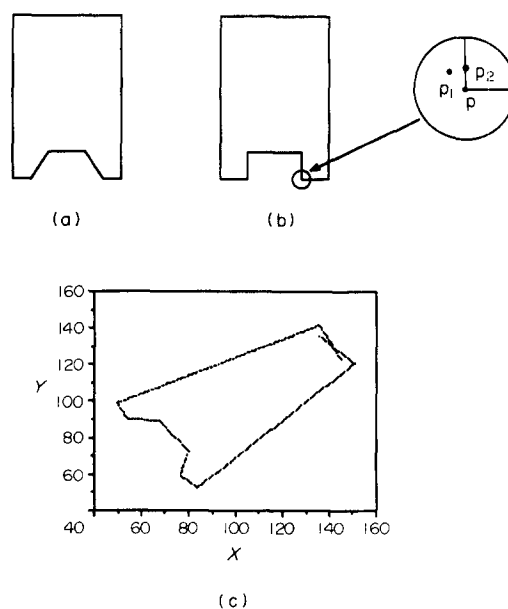


Fig. 9. Shape recovery of convex–concave shapes.

(c) For some other convex–concave shapes (e.g. Fig. 9(b)), this criterion does not work. The reason is as follows: when the recovery process reaches the point p on Fig. 9(b), according to the above criterion, point p_1 (one of the two solutions for the intersection of the two circles) is selected as the next point on the shape’s boundary, while the correct edge point is p_2 . This mistake in recovering some of the boundary points leads to a distorted shape which is an open curve as well as a crossed one (e.g. the shape in Fig. 9(b) is recovered as the open curve in Fig. 9(c)). To prevent this situation, it is proposed that these points be detected and subsequently labeled in the process of generating the signature of a shape: e.g. by using minus signs. This is a common technique in signal processing.

Thus, based on the above considerations, the AOS shape-encoding scheme can be generally made information-preserving, and to provide one-to-one mapping. As a result, it could be used as a data-compression scheme for 2D shapes. As well, since it uniquely transforms a 2D shape to a 1D signature, the AOS signature is appropriate for shape recognition.

One last important aspect of the shape-recovery procedure that deserves to be emphasized, from a *practical* point of view, is the problem of *computational error*. This is a crucial issue in real applications (as opposed to simulated ones in which, for example, quantization error does not play an important role). Moreover, the associated problem is related to the *accumulation* of computational error resulting in a *negative* value for the discriminant of a second-order polynomial. The explanation is as follows: to estimate the coordinates of a boundary point, a second-order polynomial in terms of the variable x or y must be solved (to provide the intersection of the two circles).

Clearly, based on the discriminant of the polynomial, the number of solutions is determined. Since the two circles must have either one or two solutions (based on the relative sizes of the radii of the two circles), the discriminant must be either equal to zero or have a positive value. However, when the x or y coordinates of the two solutions are equal or very close, the discriminant becomes negative due to the accumulation of computational error. A simple *practical* measure has been used to prevent this: the discriminant for both second-order polynomials in terms of variables x and y are estimated for each individual boundary point, and the larger one is used. For example, if the value of the discriminant for the polynomial in terms of x is larger, accordingly the x coordinate is first estimated, and on that basis, the y coordinate is calculated. It has been shown experimentally that this practical scheme is effective in preventing accumulation of computational error in the process of recovering a shape from its AOS signature.

3.3. A multi-scale representation based on the AOS signature

The smoothing operation produces different results when applied at different scales (which control the extent or degree of smoothing). An alternative to the use of only one scale for operations such as smoothing, is to apply a multi-scale approach. This approach allows one to consider structural features over a continuum of scales simultaneously. A useful and important property that an encoding scheme might have is that a smoothed version of the representation be obtained through some simple operation performed on it. This property is important since it can be employed for multi-scale representation.

As was indicated in Section 3.1, a family of AOS signatures of a shape with different degrees of smoothing can be generated by increasing the length of the COS (Fig. 7). One important aspect of this multi-scale representation process is that the signature is directly smoothed, and based on that, a multi-scale representation is generated. This is in contrast to the situation with other multi-scale representation schemes where, first, the original shape must be smoothed by applying some preprocessing operation, and then, the smoothed representation (a signature with a new scale) can be generated (e.g. reference (21)). Thus, from a computational point of view, the proposed AOS signature is much faster for generating multi-scale representations.

4. MATCHING OF AOS SIGNATURES

It is shown in the Appendix that the CE of any planar shape is a shape-specific ellipse, which thus behaves as an inseparable part of the shape. Conceptually, it can be said that each shape is "accompanied" by such a characteristic ellipse. This idea suggests that two shapes can be matched by first aligning their characteristic ellipses. This process of alignment in the

image plane can be performed in two steps. First, superimpose the two shapes so that their CE centers coincide, and subsequently, rotate one of the shapes until the major/minor axes of their characteristic ellipses align. Alignment of shapes in the image plane is equivalent to superimposing their AOS signatures, recalling that the AOS signature is transformation-invariant, and that its starting point lies on the major axis (or minor axis) of the characteristic ellipse.

Conceptually, if two shapes are similar, a dissimilarity measure of their signatures is expected to achieve its global minimum within a small 1D window, ∇ , centered around the starting point of the superimposed signatures. This windowed "shift-and-match" search is necessary to allow for possible *noise-induced* displacement of the characteristic ellipse (due to the variabilities in boundary quantization, edge detection, and shape orientation). It is proposed to use the following average pointwise dissimilarity measure:

$$D(j) = \frac{1}{K} \sum_{i=0}^{K-1} (S_1(i) - S_2(i+j))^2, \quad j \in [-\nabla, \nabla] \quad (5)$$

where $S_1(i)$, $i = 0, 1, \dots, M-1$, and $S_2(i)$, $i = 0, 1, \dots, N-1$, are two shape signatures (two discrete ordered sequences), M and N are the total numbers of elements in the ordered sequences (e.g. the total number of links in the Freeman chain code), and $K = \min(M, N)$.

If the eccentricity of the CE is above a certain threshold, the shape can be considered rotationally symmetric. As a result, the starting point, as defined in Section 2.1, is not unique. Thus, the axes of the CE cannot be used for superimposition of shapes. In reference (19), Freeman proposes using min-max points of a curvature-based signature for starting-point selection. This idea can be extended and implemented for alignment of min-max points of the AOS signatures to achieve proper superimposition of the shapes to be matched. Evidently, if two shapes are similar, there is a correspondence between the min-max points of their signatures, and the dissimilarity measure is minimized by proper alignment of min-max points. One should notice that the geometrical interpretation of the min-max points of an AOS signature is as follows: a maximum extremum point corresponds to a concavity of a shape or is caused by a long linear segment, while a minimum extremum point corresponds to a corner (a vertex). In this sense, alignment of AOS signatures by using pairs of maximum (or minimum) extremum points can be considered as superimposition of edges (or vertices) of the shapes to be matched. For more details on edge-based shape alignment, the reader should refer to reference (40). Shape matching through alignment of features like edges or vertices implies searching for those pairings of maximum (or minimum) extremum points whose alignment would minimize the dissimilarity measure. To avoid considering all possible combinations, we confine the search process only to the min-max points which are dominant, i.e. having a high (or the highest) domain of support. Correspondingly, we have im-

Table 1. Distance measure performance of the improved AOS signature

Test shapes	Library shapes					
						
	4.78	12.63	14.06	9.35	94.74	13.82
	0.96	9.48	15.53	3.55	114.82	11.4
	0.125	9.29	18.13	2.26	122.58	13.87

plemented the algorithm presented in reference (41) for detection of extremum points of the AOS signatures and for ordering them in accord to their domain of support.

To evaluate the performance of the above dissimilarity measure, the following experiment was performed, based on simulated test and library (reference) shapes: the performance of the AOS dissimilarity measure is shown in Table 1. The test shapes—rotated, scaled and distorted versions of a rectangular shape—are matched against a set of library shapes. The results obtained for the dissimilarity measure show that despite the fact that most of the library shapes are quite similar, the test shapes can be identified using a simple minimum-distance rule. These results also indicate that, due to the uniqueness of the signature, geometrically dissimilar objects are classified as different.

5. EXPERIMENTAL PROCEDURE AND RESULTS

In order to test the proposed encoding and matching schemes, 35 randomly-selected manufactured objects were considered (as shown in Figs 10–12): the range of their sizes (in terms of area and perimeter length) is quite large; they represent simple and basic as well as very complex shapes (in terms of the complexity measure used in this study); as well, the eccentricity values of their CEs are well distributed. These aspects of the selected objects (shapes) can be seen in Table 2.

5.1. Generation of reference and test shapes

To generate the set of reference shapes for the set of objects, the following procedure was employed:

(1) The objects were positioned in the scene such that the major axes of their CEs would be almost horizontal, and, as well, they would be at the center of the field of view of the camera. This position is referred to as the standard reference position.

(2) The camera was located directly over the object at an approximate distance of 0.7 m.

(3) A backlit-illumination system was employed such that an image of the silhouette of an object could be acquired easily.

(4) The focal length, and the aperture size of the camera were adjusted for each object in order to get a sharp and focused image.

(5) An image was acquired and subsequently processed as follows:

- The smallest rectangle that envelops the object was determined and image preprocessing was applied to this window of interest.

- An optimal global threshold value was determined based on a non-parametric and unsupervised method of automatic threshold selection.⁽⁴²⁾ The optimal threshold was selected by a discriminant criterion to maximize the separability of the resultant classes in a grey-level image. Subsequent to the selection of the optimal threshold value, a binary image was generated.

- Erosion and dilation operators were applied to remove scattered noise in the background of the binary image.

- The image was read raster-scan-wise and a boundary point was detected. Subsequently, the boundary of the silhouette was traced and a 1D Freeman chain code was produced.^(43,44)

(6) The AOS signature of the silhouette of the object was generated based on the 1D chain code. This signature was used as a reference signature.

The above procedure represents reality in part; that is, the reference model (signature) generated is based on a relatively “ideal”, though *real*, condition, rather than on an ideal *simulated* condition (such as a CAD model). Thus, it has some degree of perspective distortion, and boundary noise due to binarization and quantization processes.

The signatures of the test shapes, on the other hand, were generated with procedures similar to those above, but with the following differences:

- The objects were randomly positioned and oriented.

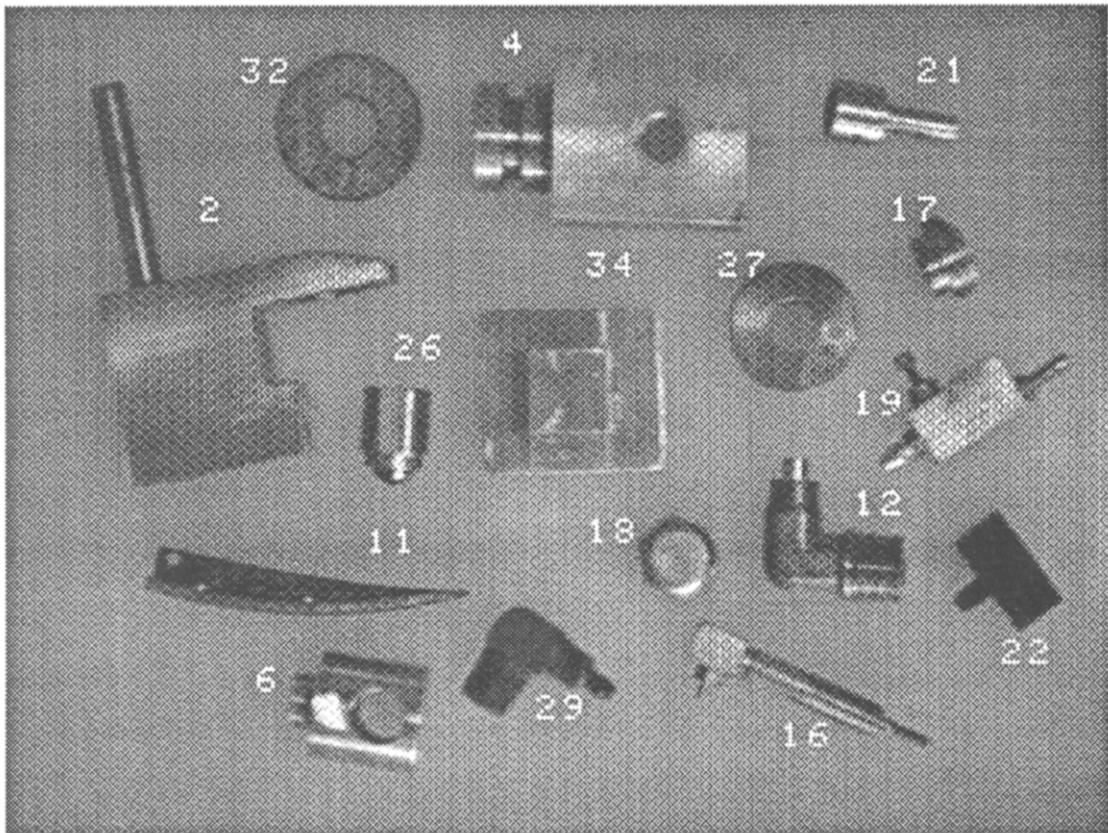


Fig. 10. A grey-level image of the manufactured objects used in the experiment.

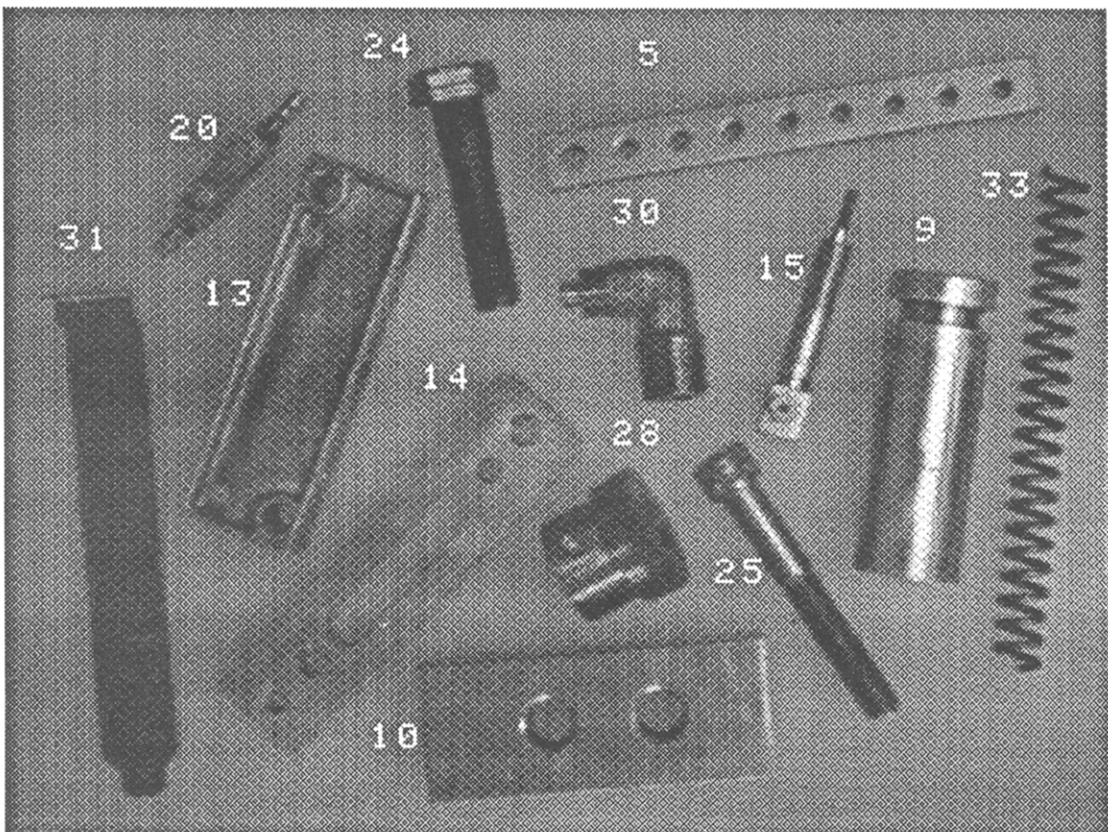


Fig. 11. A grey-level image of the manufactured objects used in the experiment.

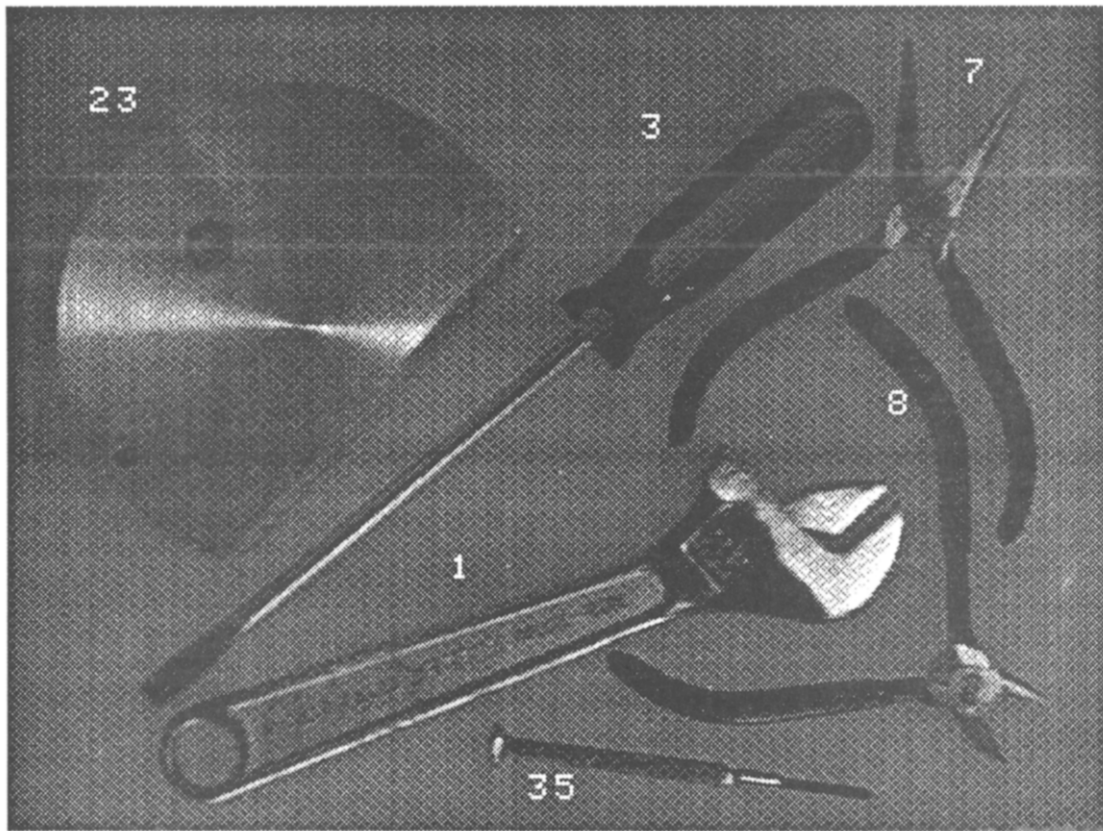


Fig. 12. A grey-level image of the manufactured objects used in the experiment.

- The focal length and aperture size of the camera were fixed (at average values) for all the test objects.
- No window of interest was employed.

Based on these differences, each shape goes through various degrees of *additional* distortion due to orientation and position (off-center) changes, relatively blurred edges, and less-contrasted imaging. As a result, in some cases, the boundary of a shape is significantly distorted, especially those with cylindrical surfaces (e.g. object number 9). These changes are manifested, for example, in the change of values of perimeter length (in terms of link units), the complexity measure, and the eccentricity of the CE of each shape as shown in Table 2.

5.2. 2D shape matching

Subsequent to the generation of AOS signatures (both the reference and test ones), the proposed matching technique was applied. In this regard, the following aspects of the process must be noted:

(1) The size of the 1D window for the "shift-and-match" search process was assumed to be 1/20 of the perimeter length of a shape. This is, generally, a relatively large window compared to the actual required size for many test shapes as can be seen in Table 2. However, it was accepted in order to provide a higher degree of confidence in the results obtained. Furthermore, the size of the window can be *objectively* determined according to some measure which is a function

of perimeter length, complexity-measure value, and eccentricity of the CEs of a set of shapes, off-line and in advance.

(2) In case of rotationally-asymmetric shapes, since the matching procedure is based on the alignment of the major and minor axes of CEs of two shapes, there exists a π -ambiguity in the alignment process. This must also be taken into account in the matching algorithm.

(3) To determine the presence of centrally symmetric shapes, the value 0.95 was used as an eccentricity threshold. This value was determined experimentally. In the set of 35 shapes under consideration, four of them are classified as centrally symmetric (shape numbers 18, 26, 27, and 32).

(4) The size of the COS for each shape was selected to be the mean value of its CE's major and minor radii.

Based on the above considerations, each *test* signature was compared with the 35 *reference* signatures. The results of the experiment on all 35 *test* shapes (signatures) are shown in Table 3. As can be seen from this table, 33 of the 35 test shapes are classified correctly. Amongst this group, three are classified correctly but with a low degree of confidence; that is, in three cases there exists a *next* closest candidate whose dissimilarity distance value is less than twice that of the first candidate (see the notes associated with Table 3). On the other hand, there are two test shapes that are misclassified through the minimum distance

Table 2. Basic data for the shapes of the 35 manufactured objects (both reference and test shapes)

Test shape No.	Perimeter length (in link unit)			CE eccentricity: $E = B/A$			Shape complexity: C			Starting point Shift ΔS
	Reference	Test	ΔP (%)	Reference	Test	ΔE	Reference	Test	ΔC	
01	1214	1110	-8.57	0.204	0.196	-0.008	56.46	59.99	3.53	0 ($W=55$)
02	1021	863	-15.48	0.645	0.656	0.011	50.80	51.21	0.41	4 ($W=43$)
03	1344	1245	-7.37	0.102	0.101	-0.001	76.92	86.61	9.69	0 ($W=62$)
04	706	612	-13.31	0.644	0.642	-0.002	21.04	22.98	1.94	1 ($W=30$)
05	839	831	-0.95	0.154	0.155	0.001	45.43	49.39	3.96	-2 ($W=41$)
06	356	356	0.0	0.838	0.819	-0.019	17.33	18.03	0.70	1 ($W=17$)
07	1530	1564	2.22	0.920	0.911	-0.009	185.89	190.15	4.26	13 ($W=76$)
08	1393	1387	-0.43	0.352	0.376	0.024	155.51	155.67	0.16	-3 ($W=69$)
09	638	615	-3.60	0.428	0.405	-0.023	23.09	26.85	3.76	-2 ($W=30$)
10	735	718	-2.31	0.477	0.468	-0.009	23.09	22.53	-0.56	-1 ($W=35$)
11	515	464	-9.90	0.160	0.165	0.005	49.05	51.34	2.29	0 ($W=23$)
12	386	395	2.33	0.578	0.584	0.006	25.26	25.74	0.48	-1 ($W=19$)
13	768	587	-23.57	0.394	0.386	-0.008	22.03	23.43	1.40	-1 ($W=29$)
14	810	694	16.7	0.328	0.327	-0.001	25.01	28.02	3.01	3 ($W=34$)
15	433	431	-0.46	0.172	0.176	0.004	47.48	48.69	1.21	0 ($W=21$)
16	476	474	-0.42	0.188	0.194	0.006	54.38	55.39	1.01	10 ($W=23$)
17	175	158	-9.71	0.648	0.659	-0.011	18.24	18.37	0.13	1 ($W=7$)
18	182	183	0.55	0.976	0.995	0.019	15.36	15.70	0.34	4 ($W=9$)
19	469	471	0.43	0.512	0.512	0.000	44.76	45.21	0.45	0 ($W=23$)
20	351	355	1.14	0.200	0.205	0.005	41.18	43.67	2.49	-2 ($W=17$)
21	273	262	-4.03	0.423	0.418	-0.005	27.59	30.44	2.85	0 ($W=13$)
22	289	276	-4.50	0.793	0.792	-0.001	22.41	24.90	2.49	-2 ($W=13$)
23	1165	1107	-4.98	0.775	0.776	0.001	15.43	16.16	0.73	5 ($W=55$)
24	493	507	2.84	0.289	0.297	0.008	38.83	40.97	2.14	-9 ($W=25$)
25	532	517	-2.82	0.175	0.180	0.005	45.34	49.11	3.77	6 ($W=25$)
26	217	195	-10.14	0.780	0.772	-0.008	16.04	16.61	0.57	-1 ($W=9$)
27	291	300	3.09	0.986	0.998	0.012	14.78	15.01	0.23	-1 ($W=14$)
28	345	318	-7.83	0.985	0.981	-0.004	16.75	17.86	1.11	3 ($W=15$)
29	332	317	-4.52	0.590	0.607	0.017	26.48	27.75	1.27	2 ($W=15$)
30	331	312	-5.74	0.590	0.607	0.017	26.49	28.03	1.54	0 ($W=15$)
31	846	735	-13.12	0.216	0.215	-0.001	34.67	38.66	3.99	0 ($W=36$)
32	312	321	2.88	0.984	0.993	0.009	14.02	14.09	0.07	-3 ($W=16$)
33	2192	1961	-10.54	0.060	0.076	0.016	866.60	591.71	-274.89	-8 ($W=109$)
34	504	493	-2.18	0.918	0.904	-0.014	15.58	17.29	1.71	-1 ($W=24$)
35	695	676	-2.73	0.075	0.76	0.001	100.46	108.63	8.17	-1 ($W=33$)
Variation	-23.57 to 16.7%			-0.023 to 0.024			-0.56 to 3.53			-9 to 13

Notes: $\Delta P(\%) = 100(P_t - P_r)/P_r$; $\Delta E = E_t - E_r$; $\Delta C = C_t - C_r$; r, reference shape; t, test shape; W , the total size of the 1D window for the "shift-and-match" process; $S^* - (W/2) < S < S^* + (W/2)$; S^* , the initial starting point (the intersection of the major axis of CE of a shape with its boundary); S , the shifted starting point; ΔS , starting point shift, $\Delta S = S^* - S$.

rule: numbers 25 and 27. In these instances, the dissimilarity caused by quantization error predominates over the geometric dissimilarity, which results in misclassification. This can be seen from the fact that the corresponding dissimilarity measure values in Table 2 are small and quite close to each other. As a result, it can be said that the matching scheme leads to a high degree of correct classification.

In order to reduce the search space, a two-level matching process is proposed: in the first level, a global measure is used to reduce the search space; in the second level, the AOS signature of a test shape is compared, through a dissimilarity measure, with the set of AOS reference signatures in the reduced search space. Two global scalar measures were tested, namely the eccentricity of the CE of each shape (which is defined as the ratio of minor and major radii), and the shape complexity (which is defined as the ratio of the square of perimeter length and the area of a shape). In Table 2, the values of these global measures are given

for all reference and test shapes. From this table, the following can be concluded:

(1) Due to the quantization process, the average variation of the perimeter length (in terms of link unit) for test shapes compared to reference shapes lies between -23.57 and 16.70%. This shows the significant effect of shape orientation on perimeter length, a factor which affects the signature as well.

(2) The variation of the eccentricity measure ranges from -0.023 to 0.024. It is noted that this value can, in general, range from 0 to 1. Thus in a sense the variation is only from -2.3 to 2.4%. As a result, it can be concluded that this measure is a very stable measure, and thus, can be used for the initial phase of a classification process. In fact, this is a direct result of the property of CE as being shape-specific. Application of this measure leads to a significant reduction in the search space. Experimental results on the 35 test shapes show that on the average, only five reference

Table 3. Experimental results for the identification of the shapes of the 35 manufactured objects based on the proposed matching scheme

Test shape No.	Closest candidate No.	MDV*	Next closest candidate		Correctly classified		Mis-classified	RNCBEM No.
			No.	MDV	LMDV	MMDV		
01	01	0.876	16	12.644	✓			8
02	02	0.194	29	93.875	✓			3
03	03	0.165	35	5.688	✓			3
04	04	0.778	26	9.136	✓			3
05	05	0.006	25	0.698	✓			7
06	06	0.134	26	4.063	✓			4
07	07	1.107	23	135.314	✓			2
08	08	0.749	19	76.013	✓			4
09	09	0.735	13	0.990		✓		3
10	10	0.076	09	1.269	✓			4
11	11	0.194	31	8.969	✓			7
12	12	0.351	30	8.024	✓			3
13	13	0.055	14	1.658	✓			4
14	14	0.054	13	2.435	✓			3
15	15	0.142	05	0.998	✓			8
16	16	0.177	25	7.485	✓			8
17	17	0.408	23	7.556	✓			3
18	18	0.165	32	1.5579	✓			4
19	19	0.147	17	51.032	✓			2
20	20	0.224	31	1.009	✓			7
21	21	0.400	24	15.725	✓			3
22	22	0.287	23	35.539	✓			4
23	23	0.380	26	7.580	✓			3
24	24	2.406	31	3.516		✓		2
			20	4.275				
			14	4.355				
25	05	0.603	25	0.702			✓	8
			15	0.806				
26	26	0.263	32	15.744	✓			4
27	32	0.128	27	0.143			✓	4
28	28	0.100	34	5.835	✓			4
29	29	0.395	12	12.262	✓			6
30	30	0.614	12	7.882	✓			6
31	31	0.022	20	1.088	✓			6
32	32	0.049	27	0.110	✓			4
33	33	4.679	35	5.117		✓		3
			05	7.627				
			25	7.824				
34	34	0.126	28	7.000	✓			2
35	35	0.045	05	3.290	✓			3

Notes: $COS = (A + B)/2$; 1D search window size = (Perimeter length)/20; MDV*, the smallest mean-distance value; MDV, the range of mean-distance values of the closest candidates, $MVD^* < MDV < 2(MVD^*)$; LMDV, large mean distance value, $LMDV > 2(MDV^*)$; MMDV, marginal mean distance value, $MVD^* < MMDV < 2(MDV^*)$; RNCBCM, reduced number of candidates based on eccentricity measure, $E_i - 0.05 < E < E_i + 0.05$.

shapes (out of 35) must be checked through matching of AOS signatures in the second phase of the matching process (see the last column of Table 3). The average size of the search space is based on the following criterion:

$$E_i - 0.05 < E < E_i + 0.05 \quad (6)$$

where E_i is the eccentricity of the CE of the test shape, and E the eccentricity of the CEs of reference shapes that are within the range given in expression (6), that is, those reference signatures considered in the second phase of the matching process.

(3) The variation for the complexity measure ranges from -0.56 to 3.53 for all shapes except shape number 33 which demonstrates to a much higher change: from 866.60 to 591.71 . These values indicate a *less stable*

property of this measure. This is expected, since the quantization and edge-detection processes lead, in some cases, to significant changes in the values of perimeter length and area. This is clearly seen for shape number 33 (Table 2).

Thus, based on the results above, it is concluded that the eccentricity of the CE of a shape is a more stable global measure, and its application in the first level of a matching scheme effectively reduces the size of the search space.

6. SUMMARY

In this paper, we addressed the problem of designing a new transformation-invariant 2D shape-encoding scheme, by which 2D standard views were transformed

into 1D signatures suitable for signal matching. In this context, the following aspects of the proposed technique were discussed: the 3D based AOS encoding scheme, the characteristic ellipse of a 2D shape and its shape-specific property, the properties of the AOS signature, a matching scheme for AOS signatures based on a dissimilarity measure, and the eccentricity of the CE of a shape as a global measure for reduction of search space. In order to test the proposed encoding and matching techniques, 35 manufactured objects were considered. The results obtained show that the AOS signature encoding scheme and the two-level matching technique are quite effective and reliable in the process of recognition of manufactured objects.

REFERENCES

1. R. Safaee-Rad, B. Benhabib, K. C. Smith and Z. Zhou, Pre-marking methods for 3D object recognition, *IEEE Proc. Int. Conf. on Systems, Man, and Cybernetics*, Cambridge, Massachusetts, Vol. II, pp. 592–595, November (1989).
2. R. Safaee-Rad, An active-vision system for 3D-object recognition in robotic assembly workcells, Ph.D. Dissertation, University of Toronto, Toronto, Ontario, May (1991).
3. T. Pavlidis, A review of algorithms for shape analysis, *Comput. Vision Graphics Image Process.* 7, 243–258 (1978).
4. T. Pavlidis, Algorithms for shape analysis of contours and waveforms, *IEEE Trans. Pattern Analysis Mach. Intell.* PAMI-2(4), 301–312 (July 1980).
5. S. Marshall, Review of shape coding techniques, *Image Vision Computing* 7(4), 281–294 (November 1989).
6. I. Tchoukanov, R. Safaee-Rad, B. Benhabib and K. C. Smith, The angle-of-sight signature for 2D shape analysis, *IEEE Proc. Int. Conf. on Acoustics, Speech, and Signal Processing*, Toronto, Ontario, Vol. 4, pp. 2461–2464, 14–17 May (1991).
7. J. J. Hwang and E. L. Hall, Scene representation using the adjacency matrix and sampled shapes of regions, *IEEE Proc. Computer Society Conf. on Pattern Recognition and Image Processing*, Chicago, Illinois, pp. 250–261, May–June (1978).
8. R. L. Kashyap and R. Chellappa, Stochastic models for closed boundary analysis: representation and reconstruction, *IEEE Trans. Inf. Theory* IT-27(5), 627–637 (September 1981).
9. S. R. Dubois and F. H. Glanz, An autoregressive model approach to two-dimensional shape classification, *IEEE Trans. Pattern Analysis Mach. Intell.* PAMI-8(1), 55–66 (January 1986).
10. H. Freeman, Shape description via the use of critical points, *IEEE Proc. Computer Society Conf. on Pattern Recognition and Image Processing*, Troy, New York, pp. 168–174, June (1977).
11. P. F. Singer and R. Chellappa, Classification of boundaries on the plane using stochastic models, *IEEE Proc. Computer Society Conf. on Computer Vision and Pattern Recognition*, Washington, DC, pp. 146–147, June (1983).
12. N. M. Marinovic and G. Eichmann, Feature extraction and pattern classification in space-spatial frequency domain, *SPIE Proc. Intelligent Robots and Computer Vision*, Cambridge, Massachusetts, Vol. 579, pp. 19–26, September (1985).
13. L. Gupta and M. D. Srinath, Contour sequence moments for the classification of closed planar shapes, *Pattern Recognition* 20, 267–272 (1987).
14. K.-B. Eom and J. Park, Recognition of shapes by statistical modeling of centroidal profile, *IEEE Proc. 10th Int. Conf. on Pattern Recognition*, Atlantic City, New Jersey, Vol. I, pp. 860–864, June (1990).
15. F. P. Kuhl and C. R. Giardina, Elliptical Fourier features of a closed contour, *Comput. Graphics Image Process.* 18, 236–258 (1982).
16. E. Persoon and K. S. Fu, Shape discrimination using Fourier descriptors, *IEEE Trans. Syst. Man Cybern.* SMC-7, 170–179 (March 1977).
17. S. Marshall, Data compression using image contours, *SPIE Proc. Intelligent Robots and Computer Vision*, Cambridge, Massachusetts, Vol. 579, pp. 47–52, September (1985).
18. C. T. Zahn and R. Z. Roskies, Fourier descriptors for plane closed curves, *IEEE Trans. Computers* C-21(3), 269–281 (March 1972).
19. H. Freeman, Use of incremental curvature for describing and analyzing two-dimensional shape, *IEEE Proc. Computer Society Conf. on Pattern Recognition and Image Processing*, Chicago, Illinois, pp. 437–444, August (1979).
20. W. Geisler, A vision system for shape and position recognition of industrial parts, *Proc. Int. Conf. on Robot Vision and Sensory Controls*, Germany, pp. 253–262 (1982).
21. F. Mokhtarian and A. Mackworth, Scale-based description and recognition of planar curves and two-dimensional shapes, *IEEE Trans. Pattern Analysis Mach. Intell.* PAMI-8(1), (January 1986).
22. D. Cyganski, J. A. Orr, T. A. Cott and R. J. Dodson, Development, implementation, testing, and application of an affine transform invariant curvature function, *First Int. Conf. on Computer Vision*, pp. 496–500, June (1987).
23. D. Vernon, Two-dimensional object recognition using partial contours, *Image Vision Computing* 5(1), 21–27 (February 1987).
24. P. J. Nahin, The theory and measurement of a silhouette descriptor for image pre-processing and recognition, *Pattern Recognition* 6, 85–95 (1974).
25. J. O'Rourke and R. Washington, Curve similarity via signature, *Computational Geometry*, G. T. Toussaint, ed., pp. 295–317 (1985).
26. J. O'Rourke, The signature of a planar shape, *SIAM J. Comput.* 15(1), 34–51 (February 1986).
27. D. J. H. Moore and D. J. Parker, Analysis of global pattern features, *Pattern Recognition* 6, 149–164 (1974).
28. S. P. Smith and A. K. Jain, Chord distribution for shape matching, *Comput. Graphics Image Process.* 20, 259–265 (December 1982).
29. D. Casasent and W.-T. Chang, Generalized chord transformation for distortion-invariant optical pattern recognition, *Appl. Optics* 22(14), 2087–2094 (15 July 1983).
30. Z. You and A. K. Jain, Performance evaluation of shape matching via chord length distribution, *Comput. Graphics Image Process.* 20, 185–198 (1984).
31. D. Casasent and W.-T. Chang, Parameter estimation and in-plane distortion invariant chord processing, *SPIE Proc. Intelligent Robots and Computer Vision*, Cambridge, Massachusetts, Vol. 579, pp. 2–10, September (1985).
32. R. Safaee-Rad, B. Benhabib, K. C. Smith and K. M. Ty, Position, rotation, and scale-invariant recognition of two-dimensional objects using a gradient coding scheme, *IEEE Proc. Pacific Rim Conf. on Communications, Computers, and Signal Processing*, Victoria, BC, pp. 306–311, June (1989).
33. C.-S. Ho, Precision of digital vision systems, *IEEE Trans. Pattern Analysis Mach. Intell.* PAMI-5(6), 593–601 (November 1983).
34. F. C. A. Groen and P. W. Verbeek, Freeman-code probabilities of object boundary quantized contours, *Comput. Graphics Image Process.* 7, 391–402 (1978).
35. B. Shahraray and D. J. Anderson, Uniform resampling of digitized contours, *IEEE Trans. Pattern Analysis Mach. Intell.* PAMI-7(6), 674–681 (November 1985).

36. D. H. Ballard, Generalizing the Hough transform to detect arbitrary shapes, *Pattern Recognition* **13**, 111–122 (1981).
37. Y. Liao, A two-stage method for fitting conic arcs and straight-line segments to digitized contours, *IEEE Proc. Int. Conf. on Pattern Recognition and Image Processing*, pp. 224–229 (1981).
38. A. Mitche and J. K. Aggarwal, Contour registration and shape-specific points for shape matching, *Comput. Vision Graphics Image Process.* **22**, 396–408 (1983).
39. R. Safaei-Rad, K. C. Smith, B. Benhabib and I. Tchoukanov, Application of moment and Fourier descriptors to the accurate estimation of elliptical shape parameters, *IEEE Proc. Int. Conf. on Acoustics, Speech, and Signal Processing*, Toronto, Ontario, Vol. 4, pp. 2465–2468, May (1991).
40. R. L. Kashyap and B. J. Oomen, A geometrical approach to polygonal dissimilarity and shape matching, *IEEE Trans. Pattern Analysis Mach. Intell.* **PAMI-4**(6), 649–654 (November 1982).
41. Cho-Huak Teh and R. T. Chin, A scale-independent dominant point detection algorithm, *Proc. Int. Conf. on Computer Vision and Pattern Recognition*, pp. 229–234, June (1988).
42. N. Otsu, Threshold selection method from gray-level histograms, *IEEE Trans. Syst. Man Cybern.* **SMC-9**(1), 62–66 (January 1979).
43. H. Freeman, Computer processing of line drawing images, *Comput. Surveys* **6**(1), 57–98 (March 1974).
44. P. W. Kitchin and A. Pugh, Processing of binary images, *Robot Vision*, A. Pugh, ed., pp. 21–42 (1983).

APPENDIX. PROOF OF THE SHAPE-SPECIFIC PROPERTY OF THE CHARACTERISTIC ELLIPSE

In order to show that the CE is shape-specific under the planar transformations (i.e. translation, rotation, and scale change), it must be proven that all five basic parameters of the CE (i.e. the center coordinates (X_0, Y_0) , the orientation (Θ) , and the major and minor radii (A, B)) are shape-specific. These parameters are expressed as follows:⁽³⁹⁾

$$\begin{aligned}
 X_0 &= A_0 + x_s \\
 Y_0 &= C_0 + y_s \\
 \Theta &= \frac{1}{2} \arctan \left[\frac{b}{a-c} \right] \\
 A^2 &= \left[\frac{2f}{b^2 - 4ac} \right] [(c+a) + \sqrt{((c-a)^2 + b^2)}] \\
 B^2 &= \left[\frac{2f}{b^2 - 4ac} \right] [(c+a) - \sqrt{((c-a)^2 + b^2)}] \quad (A1)
 \end{aligned}$$

where

$$\begin{aligned}
 a &= c_1^2 + d_1^2 \\
 b &= -2(a_1 c_1 + b_1 d_1) \\
 c &= a_1^2 + b_1^2 \\
 f &= -(a_1 d_1 - b_1 c_1)^2 \quad (A2)
 \end{aligned}$$

and

$$\begin{aligned}
 A_0 &= \frac{1}{T} \sum_{p=1}^K \frac{\Delta x_p}{2\Delta t_p} (t_p^2 - t_{p-1}^2) \\
 C_0 &= \frac{1}{T} \sum_{p=1}^K \frac{\Delta y_p}{2\Delta t_p} (t_p^2 - t_{p-1}^2) \\
 a_1 &= \frac{T}{2\pi^2} \sum_{p=1}^K \frac{\Delta x_p}{\Delta t_p} \left[\cos \frac{2\pi t_p}{T} - \cos \frac{2\pi t_{p-1}}{T} \right]
 \end{aligned}$$

$$\begin{aligned}
 b_1 &= \frac{T}{2\pi^2} \sum_{p=1}^K \frac{\Delta x_p}{\Delta t_p} \left[\sin \frac{2\pi t_p}{T} - \sin \frac{2\pi t_{p-1}}{T} \right] \\
 c_1 &= \frac{T}{2\pi^2} \sum_{p=1}^K \frac{\Delta y_p}{\Delta t_p} \left[\cos \frac{2\pi t_p}{T} - \cos \frac{2\pi t_{p-1}}{T} \right] \\
 d_1 &= \frac{T}{2\pi^2} \sum_{p=1}^K \frac{\Delta y_p}{\Delta t_p} \left[\sin \frac{2\pi t_p}{T} - \sin \frac{2\pi t_{p-1}}{T} \right]. \quad (A3)
 \end{aligned}$$

In the above equations, Δx_p and Δy_p represent the lengths of the projections of the linear link p on the x and y axes, respectively, $\Delta t_p = t_p - t_{p-1}$ is the required time to trace the link p at a constant speed, t_p and t_{p-1} are the required time to trace the contour from the starting point to the links p and $p-1$, respectively, T the total time required to trace the whole contour at a constant speed, and x_s and y_s are the coordinates of the starting point on the contour.

Translation

Under planar translation (Δx and Δy), it must be shown that Θ , A , and B remain unchanged, while the center coordinates of the CE (X_0, Y_0) are translated, with the amount of translation equal to Δx and Δy respectively.

Under translations Δx and Δy , the terms T , Δx_p , Δy_p , Δt_p , t_p and t_{p-1} do not change. As a result, the variables A_0 , C_0 , a , b , c , and f remain unchanged. Thus, the three parameters Θ , A , and B do not change either. For the other two parameters, X_0 and Y_0 , the proof proceeds as follows: the translated X_0 coordinate (X'_0) is expressed as

$$X'_0 = A'_0 + x'_s \quad (A4)$$

But, as was indicated earlier, $A'_0 = A_0$; furthermore, the x coordinate of the starting point is translated, $x'_s = x_s + \Delta x$. Thus

$$X'_0 = A_0 + x_s + \Delta x = X_0 + \Delta x. \quad (A5)$$

A similar result can be obtained for the translated Y_0 coordinate (Y'_0)

$$Y'_0 = B_0 + y_s + \Delta y = Y_0 + \Delta y.$$

Rotation

Under planar rotation δ , it must be shown that the parameters A and B remain unchanged, while the other three parameters Θ , X_0 , and Y_0 change into the following:

$$\begin{aligned}
 \Theta' &= \Theta - \delta \\
 X'_0 &= X_0 \cos \delta + Y_0 \sin \delta \\
 Y'_0 &= -X_0 \sin \delta + Y_0 \cos \delta. \quad (A6)
 \end{aligned}$$

For the CE center coordinates, the proof is as follows: let

$$X'_0 = A'_0 + x'_s \quad (A7)$$

where

$$x'_s = x_s \cos \delta + y_s \sin \delta. \quad (A8)$$

For A'_0 , the following expression can be derived based on the fact that the only term in A_0 (equation (A3)) which changes under rotation, is Δx_p :

$$\begin{aligned}
 A'_0 &= \frac{1}{T} \sum_{p=1}^K \frac{\Delta x'_p}{2\Delta t_p} (t_p^2 - t_{p-1}^2) \\
 &= \frac{1}{T} \sum_{p=1}^K \frac{1}{2\Delta t_p} (\Delta x_p \cos \delta + \Delta y_p \sin \delta) (t_p^2 - t_{p-1}^2) \\
 &= \left[\frac{1}{T} \sum_{p=1}^K \frac{\Delta x_p}{2\Delta t_p} (t_p^2 - t_{p-1}^2) \right] \cos \delta \\
 &\quad + \left[\frac{1}{T} \sum_{p=1}^K \frac{\Delta y_p}{2\Delta t_p} (t_p^2 - t_{p-1}^2) \right] \sin \delta \\
 &= A_0 \cos \delta + C_0 \sin \delta. \quad (A9)
 \end{aligned}$$

Using equations (A8) and (A9), equation (A7) would be

$$\begin{aligned} X'_0 &= (A_0 \cos \delta + C_0 \sin \delta) + x_s \cos \delta + y_s \sin \delta \\ &= (A_0 + x_s) \cos \delta + (C_0 + y_s) \sin \delta \\ &= X_0 \cos \delta + Y_0 \sin \delta. \end{aligned} \quad (\text{A10})$$

Following the above mathematical reasoning, a similar result can be obtained for Y'_0 ,

$$Y'_0 = -X_0 \sin \delta + Y_0 \cos \delta.$$

For the other three parameters (i.e. Θ , A , and B), a set of expressions for the coefficients a, b, c , and f under rotation (a', b', c' , and f') must first be derived. In order to do so, as well, a set of expressions for the variables a_1, b_1, c_1 , and d_1 under rotation (a'_1, b'_1, c'_1 , and d'_1) must be obtained:

$$\begin{aligned} a'_1 &= \frac{T}{2\pi^2} \sum_{p=1}^K \frac{\Delta x'_p}{\Delta t_p} \left[\cos \frac{2\pi t_p}{T} - \cos \frac{2\pi t_{p-1}}{T} \right] \\ &= \frac{T}{2\pi^2} \sum_{p=1}^K \frac{1}{\Delta t_p} (\Delta x_p \cos \delta + \Delta y_p \sin \delta) \left[\cos \frac{2\pi t_p}{T} - \cos \frac{2\pi t_{p-1}}{T} \right] \\ &= \left[\frac{T}{2\pi^2} \sum_{p=1}^K \frac{\Delta x_p}{\Delta t_p} \left[\cos \frac{2\pi t_p}{T} - \cos \frac{2\pi t_{p-1}}{T} \right] \right] \cos \delta \\ &\quad + \left[\frac{T}{2\pi^2} \sum_{p=1}^K \frac{\Delta y_p}{\Delta t_p} \left[\cos \frac{2\pi t_p}{T} - \cos \frac{2\pi t_{p-1}}{T} \right] \right] \sin \delta \\ &= a_1 \cos \delta + c_1 \sin \delta. \end{aligned} \quad (\text{A11})$$

Similarly

$$\begin{aligned} b'_1 &= b_1 \cos \delta + d_1 \sin \delta \\ c'_1 &= -a_1 \sin \delta + c_1 \cos \delta \\ d'_1 &= -b_1 \sin \delta + d_1 \cos \delta. \end{aligned} \quad (\text{A12})$$

Based on equations (A11) and (A12), the following expressions can be derived:

$$\begin{aligned} a' &= a_1^2 \sin^2 \delta + c_1^2 \cos^2 \delta - 2a_1 c_1 \sin \delta \cos \delta + b_1^2 \sin^2 \delta \\ &\quad + d_1^2 \cos^2 \delta - 2b_1 d_1 \sin \delta \cos \delta \\ b' &= -2(-a_1^2 \sin \delta \cos \delta - a_1 c_1 \sin^2 \delta + a_1 c_1 \cos^2 \delta \\ &\quad + c_1^2 \sin \delta \cos \delta - b_1^2 \sin \delta \cos \delta - b_1 d_1 \sin^2 \delta \\ &\quad + b_1 d_1 \cos^2 \delta + d_1^2 \sin \delta \cos \delta) \\ c' &= a_1^2 \cos^2 \delta + c_1^2 \sin^2 \delta + 2a_1 c_1 \sin \delta \cos \delta \\ &\quad + b_1^2 \cos^2 \delta + d_1^2 \sin^2 \delta + 2b_1 d_1 \sin \delta \cos \delta \\ f' &= -(a_1 d_1 - b_1 c_1)^2. \end{aligned} \quad (\text{A13})$$

Using equations (A13), it can be shown that

$$\begin{aligned} (c' - a')^2 + b'^2 &= (c - a)^2 + b^2 \\ b'^2 - 4a'c' &= b^2 - 4ac \\ c' + a' &= c + a \\ f' &= f. \end{aligned}$$

Thus

$$\begin{aligned} A'^2 &= A^2 \\ B'^2 &= B^2 \end{aligned}$$

which shows that under rotation, the CE radii A' and B' do not change, as was expected to be proved.

For the orientation parameter, to simplify the process, the proof can be started from the result and proceeds backward; that is, using the following relation:

$$\tan 2\Theta' = \tan(2\Theta - 2\delta) = \frac{\tan 2\Theta - \tan 2\delta}{1 + \tan 2\Theta \tan 2\delta} \quad (\text{A14})$$

and knowing that

$$\tan 2\Theta = \frac{b}{a - c} \quad (\text{A15})$$

and

$$\tan 2\Theta' = \frac{b'}{a' - c'} \quad (\text{A16})$$

the following must be proved:

$$j = \frac{b' \cos 2\delta + (a' - c') \sin 2\delta}{(a' - c') \cos 2\delta - b' \sin 2\delta} = \frac{b}{a - c} \quad (\text{A17})$$

To prove equation (A17), the following relations are first using equation (A13):

$$\begin{aligned} a' - c' &= -a_1^2 \cos 2\delta + c_1^2 \cos 2\delta - 2a_1 c_1 \sin 2\delta \\ &\quad - b_1^2 \cos 2\delta - d_1^2 \cos 2\delta - 2b_1 d_1 \sin 2\delta \\ b' &= a_1^2 \sin 2\delta - c_1^2 \sin 2\delta - 2a_1 c_1 \cos 2\delta \\ &\quad + b_1^2 \sin 2\delta - d_1^2 \sin 2\delta - 2b_1 d_1 \cos 2\delta. \end{aligned} \quad (\text{A18})$$

Based on equations (A18), then, it can be proved that

$$\begin{aligned} b' \cos 2\delta + (a' - c') \sin 2\delta &= -2(a_1 c_1 + b_1 d_1) \\ (a' - c') \cos 2\delta - b' \sin 2\delta &= (c_1^2 + d_1^2) - (a_1^2 + b_1^2). \end{aligned} \quad (\text{A19})$$

Thus

$$j = \frac{-2(a_1 c_1 + b_1 d_1)}{(c_1^2 + d_1^2) - (a_1^2 + b_1^2)} \quad (\text{A20})$$

Using equations (A2), (A20) is simplified to

$$j = \frac{b}{a - c} \quad (\text{A21})$$

which proves that

$$\Theta' = \Theta - \delta.$$

Scale change

For scale change, the following must be proved:

$$\begin{aligned} X'_0 &= k X_0 \\ Y'_0 &= k Y_0 \\ \Theta' &= \Theta \\ A' &= k A \\ B' &= k B. \end{aligned} \quad (\text{A22})$$

For center coordinates, the proof proceeds as follows: let

$$X'_0 = A'_0 + x'_s.$$

But A'_0 is simplified to

$$\begin{aligned} A'_0 &= \frac{1}{T'} \sum_{p=1}^K \frac{\Delta x'_p}{2\Delta t'_p} (t_p'^2 - t_{p-1}'^2) \\ &= \frac{1}{kT} \sum_{p=1}^K \frac{k\Delta x_p}{k2\Delta t_p} (k^2 t_p^2 - k^2 t_{p-1}^2) \\ &= k A_0 \end{aligned} \quad (\text{A23})$$

and x'_s is equal to

$$x'_s = k x_s.$$

Thus

$$X'_0 = k X_0. \quad (\text{A24})$$

Similarly

$$Y'_0 = k Y_0. \quad (\text{A25})$$

For the other three parameters (Θ , A , and B), first, a set of expressions for a'_1, b'_1, c'_1 , and d'_1 must be derived. a'_1 can be written as

$$\begin{aligned} a'_1 &= \frac{T'}{2\pi^2} \sum_{p=1}^K \frac{\Delta x'_p}{\Delta t'_p} \left[\cos \frac{2\pi t'_p}{T'} - \cos \frac{2\pi t'_{p-1}}{T'} \right] \\ &= \frac{kT}{2\pi^2} \sum_{p=1}^K \frac{k\Delta x_p}{k\Delta t_p} \left[\cos \frac{2\pi k t_p}{kT} - \cos \frac{2\pi k t_{p-1}}{kT} \right] \\ &= k a_1. \end{aligned} \quad (\text{A26})$$

Similarly

$$\begin{aligned} b'_1 &= k b_1 \\ c'_1 &= k c_1 \\ d'_1 &= k d_1. \end{aligned} \quad (\text{A27})$$

Based on equations (A26) and (A27), the following can be obtained:

$$\begin{aligned} a' &= k^2 a \\ b' &= k^2 b \\ c' &= k^2 c \\ f' &= k^4 f. \end{aligned} \quad (\text{A28})$$

Thus

$$\begin{aligned} \Theta' &= \frac{1}{2} \arctan \left[\frac{b'}{a' - c'} \right] = \frac{1}{2} \arctan \left[\frac{k^2 b}{k^2 a - k^2 c} \right] \\ &= \frac{1}{2} \arctan \left[\frac{b}{a - c} \right] = \Theta \end{aligned} \quad (\text{A29})$$

and

$$\begin{aligned} A'^2 &= \left[\frac{2f'}{b'^2 - 4a'c'} \right] [(c' + a') + \sqrt{((c' - a')^2 + b'^2)}] \\ &= \left[\frac{2fk^4}{(b^2 - 4ac)k^4} \right] [k^2(c + a) + \sqrt{(k^4(c - a)^2 + k^4 b^2)}] \\ &= k^2 A^2. \end{aligned} \quad (\text{A30})$$

Similarly

$$B'^2 = k^2 B^2. \quad (\text{A31})$$

Relations (A24), (A25), (A29), (A30), and (A31) prove what is expected under scale change transformation.

Based on the totality of the above proof, it can be concluded that the CE is shape-specific.

About the Author—IVO TCHOUKANOV has a M.Sc. degree in computer science engineering from the Technical University of Sofia, Bulgaria. Since 1989 he has been a research associate in the Department of Electrical Engineering at the University of Toronto. His research interests include computer vision, scene understanding and their applications to industry automation and automatic guidance systems.

About the Author—REZA SAFAEE-RAD received the B.Sc. degree in applied mathematics from the California State University, U.S.A., the B.A.Sc. degree in mechanical engineering from the Tehran Polytechnic University, Iran, the M.A.Sc. degree in electrical engineering (biomedical field) from the University of Manitoba, Canada, and the Ph.D. degree in mechanical engineering from the University of Toronto, Canada (1991). He has been the Research Director of the Computer Integrated Manufacturing Laboratory, Department of Mechanical Engineering, University of Toronto, since June 1991. He has published more than 25 papers in the areas of machine vision, computer vision, and biomedical engineering.

About the Author—KENNETH CARLESS SMITH was born in Toronto, Canada, on 8 May 1932. He received the B.A.Sc. degree in engineering physics in 1954, the M.A.Sc. degree in electrical engineering in 1956, and the Ph.D. degree in physics in 1960, all from the University of Toronto, Toronto, Canada. From 1954 to 1955 he served with Canadian National Telegraphs as a Transmission Engineer. In 1956 he joined the Computation Centre, University of Toronto, as a Research Engineer assigned to assist in the development of high-speed computers at the Digital Computer Laboratory, University of Illinois, Urbana. In 1960 he joined the staff of the Department of Electrical Engineering at the University of Toronto as an Assistant Professor. In 1961 he returned to the University of Illinois as Assistant Professor of Electrical Engineering where he became Chief Engineer of Illiac II, and then of Illiac III, and attained the rank of Associate Professor of Computer Science. In 1965 he returned to Toronto, where he is Professor in the Departments of Electrical Engineering, Mechanical Engineering, Computer Science, and Information Science, and was Chairman of the Department of Electrical Engineering from 1976 to 1981. His research interests include analog, multiple-valued and binary circuit and systems design, instrumentation in manufacturing, and computer architectures emphasizing parallelism and reliability. He is the co-author with A. S. Sedra of *Microelectronic Circuits*, HRW/Saunders College Publishing, now in its third edition. As well, he is an advisor to several international companies in the area of new-product development and education. He has participated widely in technical and professional organizations, including the Institute of Electrical and Electronic Engineers (IEEE), the Canadian Society for Electrical Engineers (CSEE) and the Canadian Society for Professional Engineers (CSPE) including, since 1974, membership on the Executive Committee of the International Solid-State Circuits Conference (ISSCC) as Awards Chairman and in other roles. As well, for the Technical Committee on Multiple-Valued Logic of the Computer Society of the IEEE, he is Vice-Chair for Technical Activities and Co-Program Chair of ISMVL 92 in Sendai, Japan. Since 1988 he has been President of CSPE, a Canadian professional engineering service organization. He was elected Fellow of the IEEE in 1978 for "Contributions to Digital-Circuit Design".

About the Author—BENSIYON BENHABIB is an Associate Professor of Mechanical Engineering and Electrical Engineering at the University of Toronto, Canada. His research and teaching interests are in the general area of computer-integrated manufacturing. He has published over 90 scientific and technical papers on subjects such as analysis and design of robots, robotic sensors, machine vision, workcell management, and production planning. He is a senior member of SME, and a member of ASME and CSME.